

# Ouroboros: Single-step Diffusion Models for Cycle-consistent Forward and Inverse Rendering

Shanlin Sun<sup>1\*</sup> Yifan Wang<sup>2\*</sup> Hanwen Zhang<sup>3\*</sup> Yifeng Xiong<sup>1</sup> Qin Ren<sup>2</sup>  
 Ruogu Fang<sup>4†</sup> Xiaohui Xie<sup>1†</sup> Chenyu You<sup>2†</sup>

<sup>1</sup> University of California, Irvine <sup>2</sup> Stony Brook University

<sup>3</sup> Huazhong University of Science and Technology <sup>4</sup> University of Florida

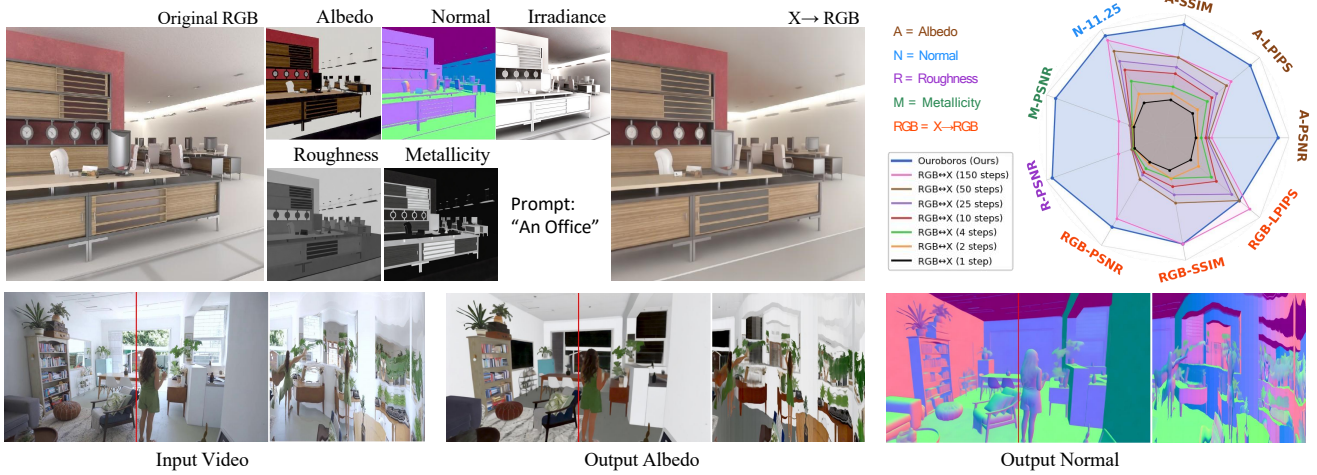


Figure 1. **Single-step Diffusion Models for Forward and Inverse Rendering in Cycle Consistency.** **Left Upper:** Ouroboros decomposes input images into intrinsic maps (albedo, normal, roughness, metallicity, and irradiance). Given these generated intrinsic maps and textual prompts, our neural forward rendering model synthesizes images closely matching the originals. **Right Upper:** We extend an end-to-end finetuning technique [47] to diffusion-based neural rendering, outperforming state-of-the-art RGB $\leftrightarrow$ X [79] in both speed and accuracy. The radar plot illustrates numerical comparisons on the InteriorVerse dataset [85]. **Bottom:** Our method achieves temporally consistent video inverse rendering without specific finetuning on video data.

## Abstract

While multi-step diffusion models have advanced both forward and inverse rendering, existing approaches often treat these problems independently, leading to cycle inconsistency and slow inference speed. In this work, we present **Ouroboros**, a framework composed of two single-step diffusion models that handle forward and inverse rendering with mutual reinforcement. Our approach extends intrinsic decomposition to both indoor and outdoor scenes and introduces a cycle consistency mechanism that ensures coherence between forward and inverse rendering outputs. Experimental results demonstrate state-of-the-art performance across diverse scenes while achieving substantially faster inference speed compared to other diffusion-based methods. We also demonstrate that Ouroboros can transfer

to video decomposition in a training-free manner, reducing temporal inconsistency in video sequences while maintaining high-quality per-frame inverse rendering. Project Page: <https://siwensun.github.io/ouroboros-project/>

## 1. Introduction

The interdependent processes of forward and inverse rendering are fundamental to computer graphics and vision. Inverse rendering [1, 2, 57] is the problem of estimating geometric, shading, and lighting information from images, a capability essential for applications such as relighting and object insertion. This problem remains challenging due to its inherently under-constrained nature when limited to a single image under single illumination [19]. On the other hand, forward rendering is to simulate the light transport to render images given the scene’s geometry, material, and

\*Equal contribution.

†Corresponding authors.

lighting information. Traditional Physically Based Rendering (PBR) [51] requires precise geometry and lighting information, which is often difficult to reconstruct accurately through inverse rendering methods.

Recent years have witnessed substantial progress through the development of large-scale annotated synthetic datasets [39, 41, 55, 56, 61, 85] and advanced deep learning techniques. Several data-driven approaches [40, 88] have emerged to estimate per-pixel intrinsic maps using neural networks, capturing properties such as diffuse color, specular roughness, metallicity, and lighting representations. The advent of diffusion models further benefits inverse rendering capabilities [31, 42, 42, 46, 79], offering powerful priors for estimating ambiguous intrinsic properties and generating photorealistic outputs. More recently, RGB $\leftrightarrow$ X [79] proposes the first diffusion model for forward rendering that accommodates flexible combinations of input intrinsic channels. Recently, DiffusionRenderer [42] integrates the idea of RGB $\leftrightarrow$ X and Neural Gaffer [25] to video diffusion [4], achieving state-of-the-art performance in video decomposition and relighting. Despite these advances, current diffusion-based approaches exhibit two critical limitations: computational inefficiency and lack of cycle consistency across inverse and forward rendering.

To this end, we propose **Ouroboros\***, a unified framework that trains single-step diffusion models for inverse and forward rendering while enforcing cycle consistency between them. Specifically, we demonstrate that a simple end-to-end fine-tuning technique [47] can be effectively applied not only to image perception tasks (geometry, material, and lighting estimation) but also to image synthesis operations (forward rendering) while preserving competitive quality. We fine-tune our single-step inverse and forward rendering models from RGB $\leftrightarrow$ X [79] using multiple heterogeneous synthetic datasets spanning both interior [61, 85] and outdoor datasets [39] with varying available intrinsic maps [79]. This approach achieves a 50 $\times$  acceleration in inference speed while maintaining state-of-the-art performance in image decomposition and synthesis.

A significant limitation of independently trained forward and inverse models lies in their inconsistent behavior when applied sequentially, where decomposed properties often fail to accurately reconstruct the original image back. Similar to ControlNet++ [37], we implement cycle consistency in conditional image understanding and generation. Our single-step generation framework enables straightforward enforcement of cycle consistency in pixel space between inverse and forward rendering during training, similar to CycleGAN [86]. This cycle consistency mechanism facilitates the incorporation of unannotated real-world data into the training process through self-supervision, thereby reducing dependence on large-scale, high-quality, and diverse syn-

thetic renderings with paired annotations.

Beyond its primary capabilities, Ouroboros offers valuable benefits for downstream applications. We explore a simple, training-free approach to extend our image-based neural inverse rendering method to consistent long video intrinsic decomposition by flattening spatial-temporal video patches and extending 2D convolution kernels into pseudo-3D kernels. Additionally, we demonstrate promising preliminary results in fine-tuning Ouroboros for single-step diffusion-based object removal and insertion.

In summary, our contributions include:

- A state-of-the-art fast diffusion-based neural framework for inverse and forward rendering, validated across indoor and outdoor scene domains;
- A cycle consistency training methodology that ensures coherence between image decomposition and synthesis while enabling the utilization of heterogeneous synthetic datasets and unannotated real-world data;
- A training-free approach for achieving temporal stability in video applications despite training exclusively on image data.

## 2. Related Works

**Diffusion Models for Image Understanding.** Diffusion models [22, 23] excel at generating photorealistic images by reversing a learned noising process. Conditioned on inputs like text prompts [4, 14, 62, 64], they have advanced numerous vision tasks, including conditional generation [48, 54, 74, 80], image and video editing [5, 8–10, 27, 45, 72], and story generation [66, 84]. Beyond generation, diffusion models are further adapted for perception tasks like geometry estimation [15, 20, 21, 28, 73], semantic segmentation [71, 87], and pose estimation [17, 34, 68]. By reformulating these as conditional generation problems, pre-trained models can be fine-tuned to produce dense prediction maps from single images, leveraging their capacity for intricate detail. Fine-tuning pre-trained diffusion models has also become an effective strategy for achieving various image editing effects, including altering lighting conditions. DiLightNet [78] provides fine-grained control over lighting during image generation by using radiance hints to guide the diffusion process. LightIt [32] proposes an identity-preserving relighting model conditioned on an image and a target shading. Relightful Harmonization [60] manipulates the illumination of foreground objects using background conditions. Similarly, Neural Gaffer [25] relights foregrounds with target environment maps. More recently, IC-Light [81] focuses on scaling up the training of diffusion-based illumination editing models by imposing consistent light transport, ensuring illumination is modified while preserving other intrinsic image properties. These approaches often leverage techniques such as 3D rendering, Neural Radiance Fields (NeRF), and synthetic data to

\*Named after the ancient symbol of a serpent consuming its own tail.

achieve sophisticated illumination and appearance control.

**Intrinsic Decomposition** as defined by [2], separates an RGB image into components like albedo and irradiance, with modern methods also estimating factors such as roughness and normals. To improve accuracy, these methods leverage diverse inputs including human annotations [33, 69, 83], ordinal cues [6, 89], physical priors [58, 76], structural models [16], and multi-view data [52, 70, 75]. Current approaches also utilize pretrained generative models [26, 62] for extracting intrinsic images, either via latent space optimization [3], low-rank adaptations [13], or image-conditioned diffusion generative models [31, 46]. The advancement of these models is coupled with the growing availability of high-quality, large-scale synthetic datasets, including interior datasets like InteriorNet [38], OpenRooms [41], InteriorVerse [85], and Hypersim [61], as well as outdoor datasets such as MatrixCity [39]. The state-of-the-art method, RGB $\leftrightarrow$ X [79], estimates multiple intrinsic buffers using synthetic interior data. Our work builds on this foundation by fine-tuning with both interior and outdoor datasets to achieve faster, more accurate decomposition. Recently, DiffusionRenderer [42] extends similar diffusion-based inverse rendering techniques to the video domain.

**Neural Image Synthesis from Decompositions.** While state-of-the-art rendering uses Monte Carlo simulation [51], synthesizing images from intrinsic decompositions is challenging. Traditional methods require full 3D geometry and explicit light/material properties, which are absent in decomposed representations. To address this, recent work leverages neural networks to synthesize images from intrinsic buffers. Approaches include using CNNs for screen-space shading [49], employing screen-space ray methods [85], and using diffusion models to compose realistic images from intrinsic channels [79]. Our work aligns with this direction, using intrinsic maps to guide image synthesis while enforcing cycle consistency between decomposition and synthesis. Neural image relighting methods have been developed with explicit decomposition [18, 29, 32, 50, 77] or implicit representations [44, 63, 67]. DiffusionRenderer [42] takes pre-defined environment maps, instead of diffuse shading maps, as inputs to the forward rendering model, thereby supporting zero-shot image relighting by incorporating novel environment maps. ZeroComp [82] and RGB $\leftrightarrow$ X [79] both demonstrate 3D object compositing methods built upon neural rendering.

### 3. Preliminary: RGB $\leftrightarrow$ X

RGB $\leftrightarrow$ X [79] proposed a unified diffusion framework for both inverse rendering (RGB $\rightarrow$ X) and forward rendering

(X $\rightarrow$ RGB) using latent diffusion models [62] that operate in VAE [30] latent space with encoder  $\mathcal{E}$  and decoder  $\mathcal{D}$ . Their approach operates on five intrinsic channels: normal vector  $\mathbf{n} \in \mathbb{R}^{H \times W \times 3}$ , albedo  $\mathbf{a} \in \mathbb{R}^{H \times W \times 3}$ , roughness  $\mathbf{r} \in \mathbb{R}^{H \times W}$ , metallicity  $\mathbf{m} \in \mathbb{R}^{H \times W}$ , and diffuse irradiance  $\mathbf{E} \in \mathbb{R}^{H \times W \times 3}$ . The RGB $\rightarrow$ X model estimates intrinsic channels from an RGB image  $\mathbf{I} \in \mathbb{R}^{H \times W \times 3}$  by fine-tuning a pre-trained latent diffusion model with v-prediction [65]:

$$\mathbf{v}_t^{RGB \rightarrow X} = \sqrt{\bar{\alpha}_t} \epsilon - \sqrt{1 - \bar{\alpha}_t} \mathbf{z}_0^X, \quad (1)$$

where  $t$  is the diffusion time step,  $\epsilon \sim \mathcal{N}(\mathbf{0}, \mathbf{I})$  is Gaussian noise,  $\bar{\alpha}_t$  is a scalar function of  $t$ , and  $\mathbf{z}_0^X$  is the clean target latent encoding the intrinsic channels. To handle multiple output channels with a single model, they repurpose the text prompt as a switch mechanism, using fixed prompts (e.g., normal, albedo, roughness) to control which intrinsic channel is produced. The X $\rightarrow$ RGB model synthesizes RGB images from intrinsic channels, defining the clean target latent as  $\mathbf{z}_0^{RGB} = \mathcal{E}(\mathbf{I})$ . The model also employs v-prediction:

$$\mathbf{v}_t^{X \rightarrow RGB} = \sqrt{\bar{\alpha}_t} \epsilon - \sqrt{1 - \bar{\alpha}_t} \mathbf{z}_0^{RGB}, \quad (2)$$

and uses a channel dropout strategy during training to handle heterogeneous datasets:

$$\mathbf{z}_t^X = (\mathcal{P}(\mathbf{n}), \mathcal{P}(\mathbf{a}), \mathcal{P}(\mathbf{r}), \mathcal{P}(\mathbf{m}), \mathcal{P}(\mathbf{E})), \quad (3)$$

where  $\mathbf{z}_t^X$  represents the noisy latent at time step  $t$ , and  $\mathcal{P}(x) \in \mathcal{E}(x), 0$  is the dropout function. This approach allows generation from any subset of channels at inference time while maintaining a single unified model. Notably, irradiance  $\mathbf{E}$  is handled differently than other intrinsic channels in the X $\rightarrow$ RGB model; while normal, albedo, roughness, and metallicity maps are encoded through the full-resolution encoder  $\mathcal{E}$ , the irradiance is instead directly downsampled to latent resolution.

## 4. Method

Ouroborosis composed of two single-step diffusion models serving for inverse and forward rendering respectively. As illustrated in Fig. 2, the neural inverse rendering (RGB $\rightarrow$ X) predicts pixel-wise geometry, material and lighting properties from an input image. The neural forward rendering is to synthesize image from intrinsic buffers.

We describe our single-step diffusion-based inverse and forward rendering finetuning strategy in Sec. 4.1 as well as cycle training pipeline in Sec. 4.2, and discuss how we inference video data with our image-based model in Sec. 4.3.

### 4.1. Finetuning Single-Step Prediction Model

Inspired by E2E [47], we finetune pre-trained RGB $\leftrightarrow$ X diffusion models to generate high-quality intrinsic maps with a

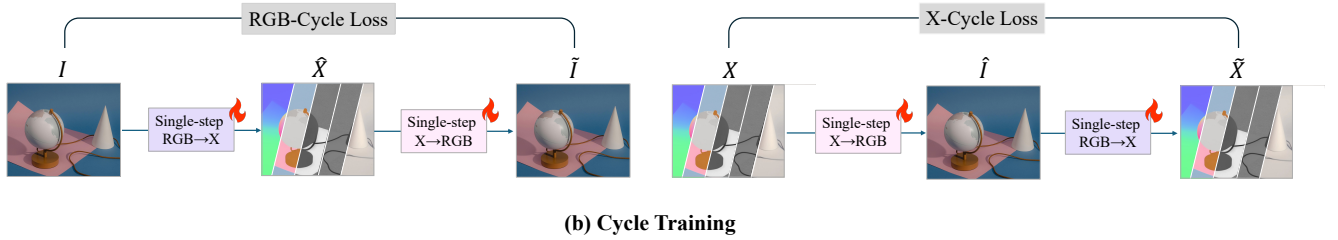
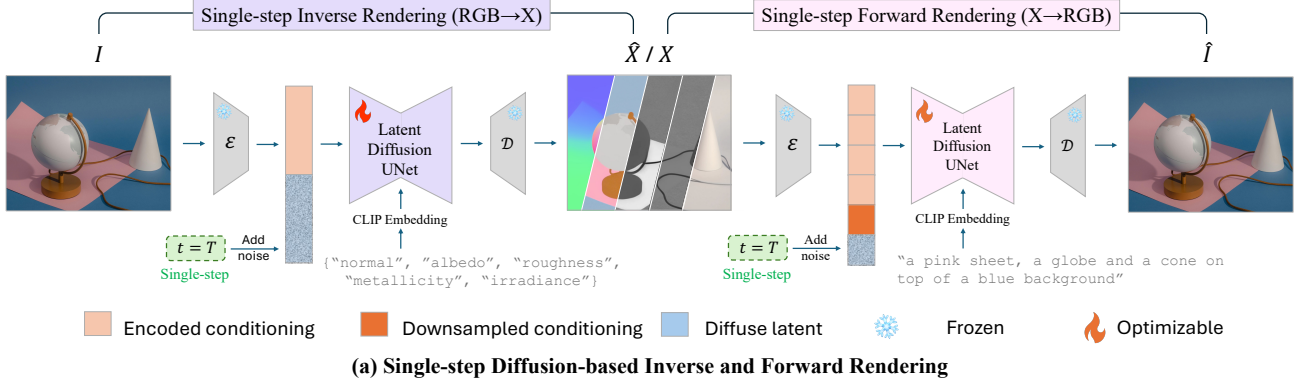


Figure 2. **Overview of Ouroboros Pipeline.** (a) presents the training pipeline of our single-step Diffusion-based inverse and forward rendering model. For inverse rendering, the model takes the image  $I$  and text prompt indicating the output intrinsic maps as input to finetune the latent diffusion UNet. For forward rendering, the model is fed with concatenated intrinsic maps along with simple image description to estimate the original image. (b) provides the overview of cycle training pipeline.

single-step inference. Given the pairwise data  $(X, I)$ , where  $I$  denotes the RGB image and  $X$  represents the set of intrinsic maps, the diffusion model uses one as a conditional input to generate the other. In our finetuning framework, most diffusion modules are frozen except for the UNet.

**Finetuning pipeline.** To enable efficient single-step prediction, we fix the timestep to  $t = T$  during training, forcing the model to learn to denoise from the most noisy state to the target in a single step. Unlike E2E [47], which uses zero noise as the initial state, we apply multi-resolution noise at timestep  $T$  to the target latent, which means our single-step model is not deterministic. This non-deterministic approach is particularly appropriate for intrinsic decomposition, which inherently admits multiple possible solutions unlike tasks such as depth or normal estimation that have more definitive ground truths.

During training, the UNet output is converted into a latent prediction using the  $\mathbf{v}$ -parameterization [65]:

$$\hat{\mathbf{z}}_0 = \sqrt{\bar{\alpha}_T} \mathbf{z}_T - \sqrt{1 - \bar{\alpha}_T} \hat{\mathbf{v}}_\theta, \quad (4)$$

where  $\hat{\mathbf{z}}_0$  is the predicted denoised latent,  $\mathbf{z}_T$  is the noised input, and  $\hat{\mathbf{v}}_\theta$  is the diffusion UNet’s output. This predicted latent is subsequently decoded into the original space via the VAE decoder for comparison with the ground truth.

**Task-specific loss functions.** We employ different loss functions tailored to each type of intrinsic map:

For normal predictions, we use a loss based on the angular difference between estimated and ground-truth normals:

$$\mathcal{L}_n = \frac{1}{N} \sum_i \arccos \frac{\mathbf{n}_i \cdot \hat{\mathbf{n}}_i}{\|\mathbf{n}_i\| \cdot \|\hat{\mathbf{n}}_i\|}, \quad (5)$$

where  $N$  represents the total number of pixels,  $\mathbf{n}_i$  denotes ground-truth normal vectors, and  $\hat{\mathbf{n}}_i$  represents predicted normal vectors.

For irradiance prediction, we apply an affine-invariant loss function [59]:

$$\mathcal{L}_E = \|\mathbf{E} - \hat{\mathbf{S}}\mathbf{E} - \mathbf{T}\|_F^2, \quad (6)$$

where  $\mathbf{E}, \hat{\mathbf{E}}$  are ground truth and predicted irradiance maps,  $\hat{\mathbf{S}}$  is a diagonal scale matrix, and  $\mathbf{T}$  contains channel-specific shift values. Parameters are determined through least-square fitting for each channel independently, accommodating the ambiguity in decomposing images into albedo and irradiance.

For all other maps, including RGB, albedo, roughness, and metallicity, we utilize the Mean Squared Error (MSE):

$$\mathcal{L}_{\{a,r,m,RGB\}} = \frac{1}{N} \sum_i |y_i - \hat{y}_i|_F^2, \quad (7)$$

where  $y_i$  represents ground-truth pixel values and  $\hat{y}_i$  corresponds to predicted values. For inverse rendering task, the



final loss is computed as the sum of these individual intrinsic map specific loss functions. For forward rendering task, the loss is  $\mathcal{L}_{RGB}$ .

**Training Data.** Due to the limited availability of datasets containing complete RGB-X pairs, we integrate multiple complementary datasets in our training pipeline. For indoor scenes, we utilize Hypersim [61] and InteriorVerse [85], following the heterogeneous data handling approach in [79] that employs channel dropout to accommodate varying availability of intrinsic channels across datasets. To ensure robustness to outdoor scenes, we incorporate MatrixCity [39], a large-scale urban dataset with photorealistic images, each accompanied by normal, albedo, metallic, and roughness maps. We randomly sample 17,000 image (with paired intrinsic maps) from each dataset.

For the forward rendering model ( $X \rightarrow RGB$ ), which requires image descriptions as conditions, we employ BLIP-2 [36] for indoor scenes and BLIP [35] for outdoor scenes. Empirically, we find that BLIP-2 provides more detailed annotations suitable for complex indoor environments, while BLIP generates more concise and accurate descriptions for outdoor scenes.

## 4.2. Cycle Training

After an initial round of finetuning, we obtain two complementary diffusion models capable of single-step inference: one for inverse rendering ( $RGB \rightarrow X$ ) and another for forward rendering ( $X \rightarrow RGB$ ). However, as these models are trained independently, they exhibit deficiencies in cycle consistency when applied sequentially. To address this limitation, we implement a cycle-consistent training approach similar to CycleGAN [86].

Given an input pair ( $\mathbf{X}, \mathbf{I}$ ), where  $\mathbf{X}$  represents intrinsic maps and  $\mathbf{I}$  denotes the RGB image, we first utilize our pre-trained single-step models to generate the corresponding outputs ( $\tilde{\mathbf{I}}, \tilde{\mathbf{X}}$ ). Subsequently, we use these generated outputs as inputs for a second inference pass, producing ( $\tilde{\tilde{\mathbf{X}}}, \tilde{\tilde{\mathbf{I}}}$ ). This enables us to define cycle consistency losses:

$$\mathcal{L}_{cycle} = \mathcal{L}_{\mathbf{X} \rightarrow \tilde{\mathbf{I}} \rightarrow \tilde{\tilde{\mathbf{X}}}} + \mathcal{L}_{\mathbf{I} \rightarrow \tilde{\mathbf{X}} \rightarrow \tilde{\tilde{\mathbf{I}}}} = |\mathbf{X} - \tilde{\tilde{\mathbf{X}}}|^2 + |\mathbf{I} - \tilde{\tilde{\mathbf{I}}}|^2 \quad (8)$$

During this additional finetuning phase, we optimize both models jointly using a combination of the task-specific losses from Section 4.1 and the cycle consistency loss. This approach serves two important purposes: (1) it improves bidirectional consistency between the inverse and forward rendering processes, and (2) it helps mitigate data scarcity issues in training the forward rendering model by leveraging the cycle structure.

**Training Data.** In addition to the annotated datasets mentioned in Section 4.1, we leverage 20,000 images sampled

from MSCOCO [43] and Flickr30k [53] datasets for cycle training. These natural image collections provide diverse visual content that helps enhance the generalization capabilities of our models.

## 4.3. Video Inference

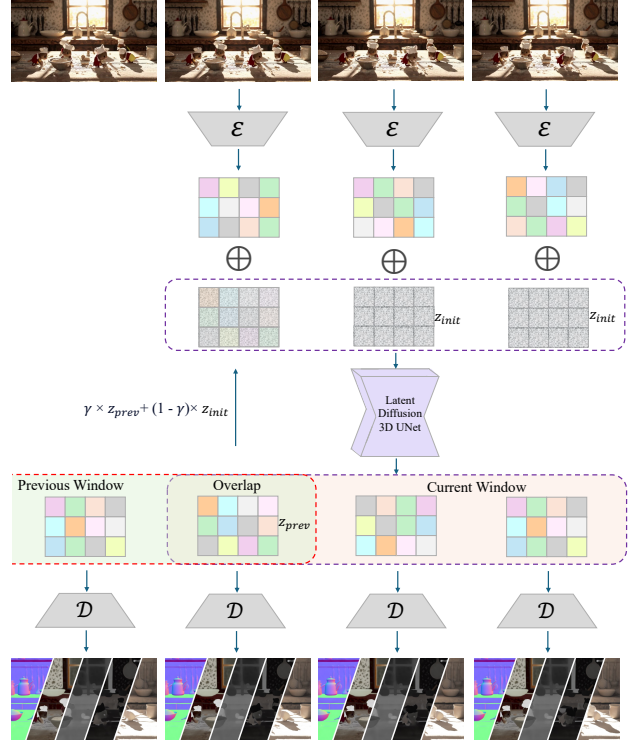


Figure 3. **Iterative Video Generation Pipeline.** Overlapping windows are processed sequentially, with latent representations from previous windows guiding the initialization of overlapping regions. In practice, the window size and overlap are larger than the figure shown.

For video inference, although training a native video diffusion model is natural, it typically requires significantly larger datasets, higher computational costs, and longer training times. Instead, we leverage our pretrained 2D diffusion model without any fine-tuning to achieve video generation capabilities.

Naive per-frame application of 2D diffusion models often results in temporal discontinuities and flickering artifacts due to the absence of inter-frame dependencies. To address this limitation, we extend our 2D architecture to handle temporal information effectively. Inspired by prior works such as VDM [24] and FLATTEN [12], we extend 2D convolution layers into a pseudo-3D architecture by replacing  $3 \times 3$  kernels with  $1 \times 3 \times 3$  kernels. Furthermore, our approach flattens patches from multiple frames and applies attention mechanisms across both spatial and temporal dimensions, improving the coherence of generated videos.

However, directly processing an entire video as input and generating the full video output in a single pass poses significant challenges due to GPU memory constraints. To overcome this limitation, we adopt an iterative inference strategy that processes videos in manageable segments. Specifically, we divide the video into overlapping windows with a fixed stride, where each segment is processed independently using our pseudo-3D diffusion model.

To maintain temporal consistency across segments, we employ a technique inspired by Lotus [21]. We take the predicted latent  $\mathbf{z}_{\text{prev}}$  of the overlap region from the previous window and apply a weighted combination with noise  $\epsilon$  using a pre-defined scale  $\gamma$ . The result serves as the initial latent input for the overlapping region in the next iteration:

$$\mathbf{z}_{\text{init}} = \gamma \cdot \mathbf{z}_{\text{prev}} + (1 - \gamma) \cdot \epsilon \quad (9)$$

where we empirically set  $\gamma = 0.1$  in our experiments. This approach ensures smooth transitions between video segments while maintaining computational efficiency. See supplementary material for a detailed demonstration of our video inference pipeline.

## 5. Experiment

### 5.1. Setup

Given that the utilization of a combination of heterogeneous datasets, and the efficacy of cycle training in mitigating the impact of imperfections in certain data, it was determined that all modalities would be utilized in the training process.

**Evaluation Datasets.** For inverse rendering, we follow the setting same as RGB $\leftrightarrow$ X [79] and utilized the HyperSim [61] test set to evaluate albedo, normal and irradiance estimation. Furthermore, to ensure the reliable evaluation for both indoor and outdoor scenes, the test sets of InteriorVerse [85] and MatrixCity [39] were employed for albedo, normal roughness and metallicity estimation as well. As for the forward rendering evaluation, the same test set of the three datasets mentioned above was applied. The intrinsic maps utilized as input varied by dataset, Hypersim used albedo, normal, and irradiance maps, while MatrixCity and InteriorVerse employed albedo, normal, roughness, and metallicity maps.

**Baseline Methods.** Since our model is finetuned based on the RGB $\leftrightarrow$ X [79] pretrain weights, we compared with it in all intrinsic map estimation tasks. For normal map estimation, we compare with state-of-the-art methods including the model proposed in Zhu et al. [85], StableNormal [73], E2E [47], and Lotus [21]. For albedo estimation, we include comparisons with models proposed by Careaga and Aksoy [7] and Kocsis et al. [31]. And for roughness and

metallicity estimation, we compare our results with models proposed by Kocsis et al. [31] and Zhu et al. [85].

**Metrics.** The evaluation of inverse rendering involved the utilization of PSNR and LPIPS metrics to assess all intrinsic maps. For albedo evaluation, scale-invariant root mean squared error (RMSE) and SSIM metrics were also incorporated. The evaluation of normal incorporated mean angular errors (Mean) and the percentage of pixels with angular errors below 11.25° thresholds. Forward rendering evaluation primarily employed PSNR, LPIPS, and SSIM metrics to assess the reconstruction quality.

## 5.2. Inverse Rendering Results

### 5.2.1. Quantitative Results

In the context of albedo and normal estimation, our approach demonstrates superior performance in nearly all metrics across three distinct datasets, with only a limited number of metrics exhibiting a second-place ranking. It is noteworthy that our method requires only a single step of inference, which further underscores its ability to produce high-quality results while significantly decrease inference time. The quantitative results are presented in detail in Tab. 1 and 2.

### 5.2.2. Qualitative Results

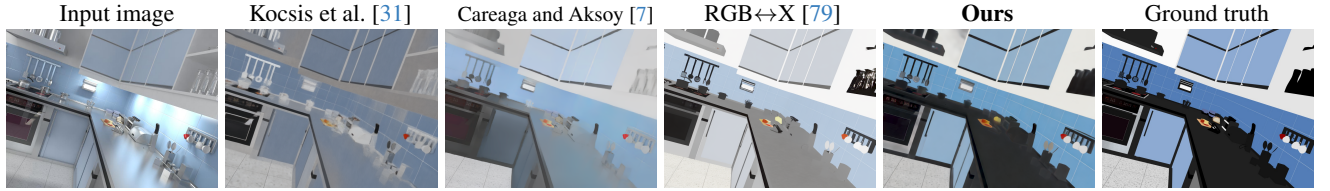
We conduct qualitative comparisons of our model’s inverse rendering capabilities across diverse indoor and outdoor scenes, against multiple baseline models, including RGB $\leftrightarrow$ X [79], as shown in ???. Due to space limitations, comparisons in outdoor scenes can be seen in the supplementary materials Fig. 7. All test scenes are explicitly excluded from our training dataset.

In terms of albedo prediction, our method achieves performance parity with RGB $\leftrightarrow$ X [79] in indoor environments while demonstrating clear advantages over other baseline models. In outdoor scenarios, our approach consistently outperforms RGB $\leftrightarrow$ X [79], particularly excelling at preserving fine details in the generation of albedo for distant objects. Moreover, our method exhibits superior ability in handling specular reflections and material properties, whereas RGB $\leftrightarrow$ X [79] tends to conflate reflection information into albedo estimation, resulting in discrepancies from the true albedo values.

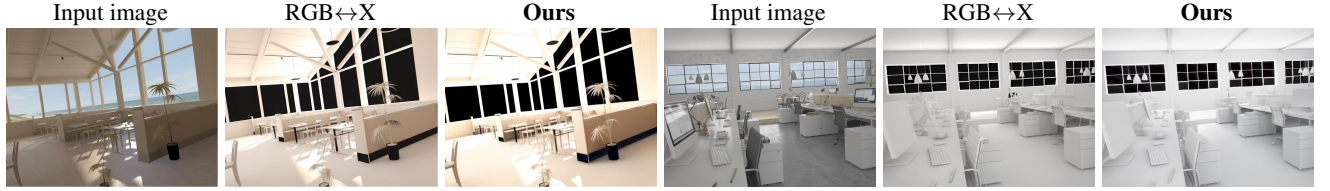
Regarding normal estimation, our method achieves performance comparable to SOTA models in indoor scenes, while in outdoor scenarios, we demonstrate more refined detail in normal prediction for smaller objects within larger scenes. Furthermore, we observe that RGB $\leftrightarrow$ X [79] tends to overestimate surface roughness in ground normal prediction, generating dense, discontinuous normals even for flat surfaces with rich color variations.

Table 1. **Albedo Prediction Results.**  $\uparrow$  ( $\downarrow$ ) means that the higher (lower), the better. We highlight the best results in **bold** and the second best with underlined format.

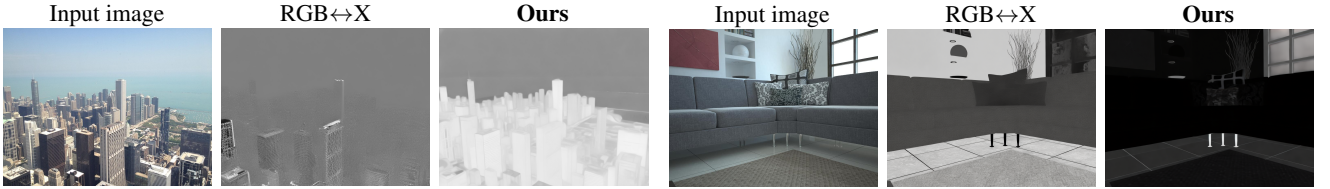
Method	Hypersim [61]				MatrixCity [85]				InteriorVerse [39]			
	PSNR $\uparrow$	LPIPS $\downarrow$	SSIM $\uparrow$	RMSE $\downarrow$	PSNR $\uparrow$	LPIPS $\downarrow$	SSIM $\uparrow$	RMSE $\downarrow$	PSNR $\uparrow$	LPIPS $\downarrow$	SSIM $\uparrow$	RMSE $\downarrow$
RGB $\leftrightarrow$ X [79]	<u>20.17</u>	<b>0.11</b>	<u>0.59</u>	<u>0.43</u>	12.61	0.26	0.53	0.50	16.17	<u>0.17</u>	0.77	0.30
Zhu et al. [85]	11.76	0.45	0.51	0.47	16.11	0.47	0.59	0.33	<u>17.19</u>	0.22	<u>0.81</u>	<u>0.29</u>
Kocsis et al. [31]	12.40	0.31	0.57	0.49	15.66	0.36	0.57	0.34	<u>14.62</u>	0.21	0.78	<u>0.37</u>
IntrinsicAnything[11]	10.39	0.51	0.50	0.55	15.62	0.49	0.57	0.55	13.12	0.32	0.72	0.43
Careaga and Aksoy [7]	12.01	0.31	0.57	0.45	<u>17.30</u>	<u>0.21</u>	<u>0.71</u>	<u>0.28</u>	15.51	0.21	0.80	0.32
<b>Ours</b>	<b>20.71</b>	<u>0.19</u>	<b>0.71</b>	<b>0.17</b>	<b>25.38</b>	<b>0.17</b>	<b>0.77</b>	<b>0.11</b>	<b>22.07</b>	<b>0.12</b>	<b>0.87</b>	<b>0.17</b>



(a) **Albedo Estimation.** Our method outperforms that of Kocsis et al. [31] and Careaga and Aksoy [7] in estimation quality. Although RGB $\leftrightarrow$ X [79] provides estimation with clear detail, its color is adversely impacted by the presence of light. Only our model achieves both image quality and correct color space.

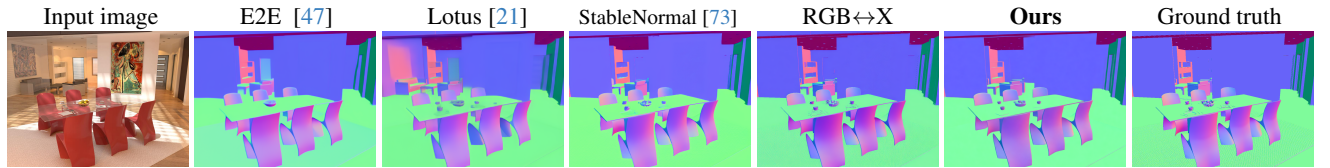


(b) **Irradiance Estimation.** Comparing to RGB $\leftrightarrow$ X, our method achieves comparable performance.



(c) **Roughness Estimation.** Our method is more representative of the surface roughness of the image rather than confusing it with the material.

(d) **Metallicity Estimation.** Our method is more effective in accentuating the textural characteristics of diverse materials.



(e) **Normal Estimation.** Our method outperforms the baseline methods in details and planar consistency.

Figure 4. **Comprehensive Visual Comparison between Baseline Models and our Ouroboros on Diverse Inverse Rendering Tasks.**

Table 2. Normal Prediction Results.

Method	Hypersim		MatrixCity		InteriorVerse	
	Mean $\downarrow$	11.25 $\circ\uparrow$	Mean $\downarrow$	11.25 $\circ\uparrow$	Mean $\downarrow$	11.25 $\circ\uparrow$
RGB $\leftrightarrow$ X [79]	17.21	73.93	23.82	49.74	12.10	80.03
Zhu et al. [85]	53.76	10.57	35.00	17.57	17.16	64.90
Lotus [21]	17.61	71.38	25.06	62.34	15.38	62.12
StableNormal[73]	16.65	<u>75.51</u>	18.18	63.28	<u>10.73</u>	<u>82.13</u>
E2E [47]	<u>16.30</u>	74.00	<b>13.91</b>	<u>67.09</u>	15.87	57.30
<b>Ours</b>	<b>11.98</b>	<b>80.71</b>	<u>18.12</u>	<b>76.21</b>	<b>9.58</b>	<b>83.54</b>

In the estimation of roughness and metallic properties, despite minor local deviations, our method demonstrates superior performance across a wider spectrum of scenarios. For indoor environments, particularly in the prediction of smooth surfaces such as tables and cabinets, our approach consistently outperforms RGB $\leftrightarrow$ X [79], which exhibits material interpretation inconsistencies. In outdoor environments, especially in the analysis of tall and distant architectural structures, RGB $\leftrightarrow$ X [79] shows substantial estimation biases, while our method maintains more consistent



Table 3. Irradiance Prediction Results.

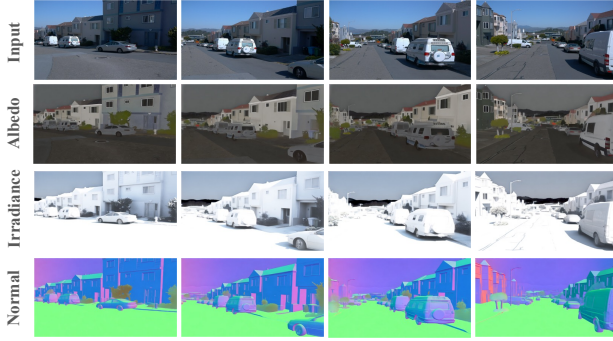
Method	Hypersim	
	PSNR $\uparrow$	LPIPS $\downarrow$
RGB $\leftrightarrow$ X	11.64	<b>0.23</b>
Du et al. [13]	9.51	0.56
<b>Ours</b>	<b>12.07</b>	<u>0.29</u>

Table 4. Roughness and Metallicity Prediction Results.

Method	MatrixCity				InteriorVerse			
	Roughness		Metallicity		Roughness		Metallicity	
	PSNR $\uparrow$	LPIPS $\downarrow$	PSNR $\uparrow$	LPIPS $\downarrow$	PSNR $\uparrow$	LPIPS $\downarrow$	PSNR $\uparrow$	LPIPS $\downarrow$
RGB $\leftrightarrow$ X [79]	<u>23.82</u>	<u>0.3655</u>	<u>6.83</u>	0.57	<u>12.07</u>	0.35	8.04	<u>0.45</u>
Zhu et al. [85]	7.0028	0.6024	4.87	<u>0.68</u>	7.51	0.51	6.45	0.78
Kocsis et al. [31]	8.4766	0.4419	10.67	0.38	11.29	<u>0.32</u>	<u>8.93</u>	0.71
<b>Ours</b>	<b>24.04</b>	<b>0.2301</b>	<b>26.32</b>	<b>0.14</b>	<b>19.56</b>	<b>0.19</b>	<b>21.96</b>	<b>0.18</b>

Table 5. Comparison between Our Ouroboros and RGB $\leftrightarrow$ X in Forward Rendering.

Method	Hypersim		MatrixCity		InteriorVerse	
	PSNR $\uparrow$	LPIPS $\downarrow$	PSNR $\uparrow$	LPIPS $\downarrow$	PSNR $\uparrow$	LPIPS $\downarrow$
RGB $\leftrightarrow$ X	16.37	<b>0.20</b>	9.24	0.30	13.70	0.33
<b>Ours</b>	<b>18.09</b>	0.25	<b>21.57</b>	<b>0.18</b>	<b>15.79</b>	<b>0.28</b>

Figure 5. **Examples of Video Inference.** Our model demonstrates the ability to process real-world scenarios.

and reliable predictions.

Our method for irradiance understanding matches the performance of RGB $\leftrightarrow$ X [79] indoors and proves more reliable in outdoor scenarios, particularly in capturing lighting on skyscraper surfaces and windows. Since our model was trained to estimate irradiance exclusively on indoor scenes in Hypersim, these results validate that our cycle-based approach successfully generalizes its understanding to new environments.

### 5.3. Forward Rendering Results

#### 5.3.1. Quantitative Results

In the forward rendering comparison, our method outperforms RGB $\leftrightarrow$ X [79] across most metrics, with particularly significant advantages in performance in MatrixCity. The quantitative results are presented in detail in Tab. 5.

#### 5.3.2. Qualitative Results

Compared to manually rendering individual image channels, which is often time and resource-intensive, we opt for an approach that performs both inverse rendering and for-

ward rendering from a single RGB input. This method not only helps us intuitively understand the forward rendering capabilities but also enables us to observe the differences between the generated RGB and the initial input RGB, allowing us to evaluate the continuity of the process.

Our experimental results demonstrate superior performance over RGB $\leftrightarrow$ X [79] in both forward rendering fidelity and consistency between input and synthesized RGB images. This advantage is particularly evident in outdoor scenes with challenging illumination conditions, where our method successfully reconstructs the original lighting distributions. Moreover, our approach exhibits enhanced capability in color fidelity preservation for distant objects compared to RGB $\leftrightarrow$ X [79]. Some results can be found at Fig. 1.

Fig. 5 showcases our model’s ability to perform video inference in real-world scenes, preserving spatial details and ensuring temporal consistency under complex lighting and material variations.

### 5.4. Ablation Study on Cycle Training

In Fig. 7, we demonstrate advantages in both inverse rendering and forward rendering compared to RGB $\leftrightarrow$ X. In inverse rendering, our Ouroboros shows better understanding of object materials such as building textures. In forward rendering, our method is significantly better at the recovery of lighting effects.

**Effects of Cycle Training.** We conducted a comparative analysis between cycle training and the combined inverse rendering and forward rendering approach for RGB-to-RGB generation. Our findings reveal that the cycle training paradigm achieves more faithful reproduction of lighting contrasts in outdoor scenes, closely matching the original image characteristics. Details can be found in Fig. 8.

**Effects of Wild Data Finetuning.** Fig. 9 showcases the effectiveness of training with wild data. For tall buildings, we can clearly see that training with wild data produces more realistic irradiance, while metallicity is more continuous, demonstrating better understanding of surface properties.



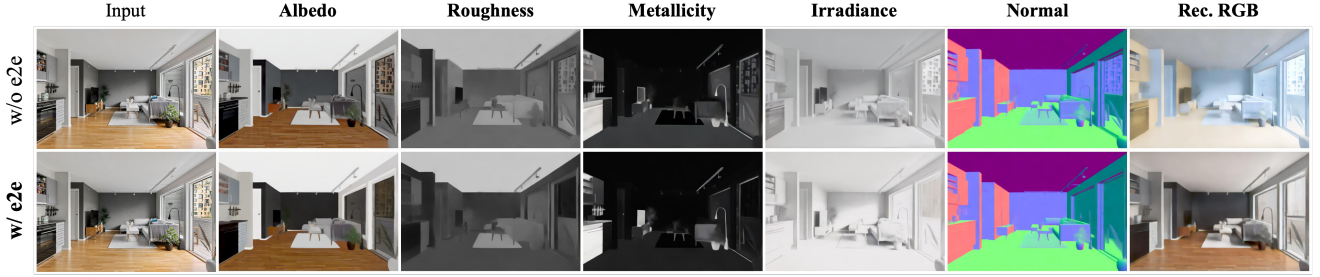


Figure 6. **Ablation Study on Cycle Training with or w/o e2e Loss.** Methods incorporating e2e loss can better understand lighting conditions and provide more continuous estimation. We can observe that the colors in the restored images are also more accurate and faithful.

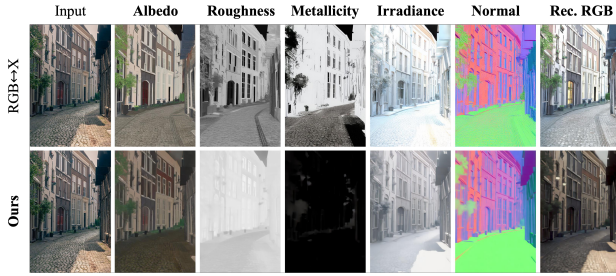


Figure 7. **Visual Comparison between RGB↔X and ours on Wild Data.** Our method demonstrates superior performance in terms of material understanding, lighting comprehension, rendering consistency.



Figure 8. **Ablation Study on Performance with or without Cycle Training.** With cycle training, the irradiance will be more sharp in details and the color of reconstruction is more consistent with the input.

**Effects of e2e Loss.** As shown in Fig. 6, we evaluated whether to use e2e loss in cycle training. We can observe that with e2e loss, there is better continuity in metallicity and irradiance predictions, and the results are more faithful to the actual physical properties and materials.

## 6. Discussion

Ouroboros explores single-step diffusion models for inverse and forward rendering, demonstrating superior performance compared to state-of-the-art methods across both indoor and outdoor scenes, as well as in image and video domains.

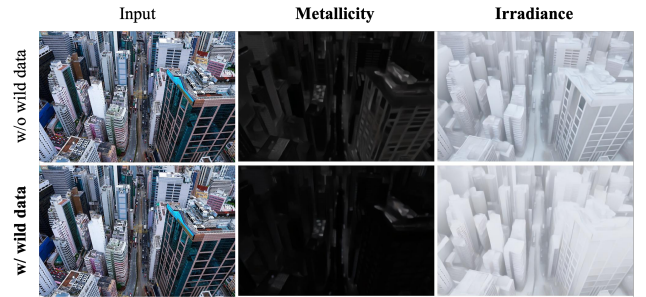


Figure 9. **Ablation Study on Cycle Training with or without Wild Data.** Training on wild data helps improve the understanding of overhead lighting and surface materials.

**Limitations and future work.** We identify training data quality and quantity as the primary bottleneck for neural rendering models. Current public datasets [61, 85] often contain unreliable intrinsic maps and typically lack accurate lighting information, limiting the model’s potential. To better support future image editing applications such as re-lighting and object insertion, we plan to curate a large-scale, diverse, high-quality synthetic dataset with full control over all components of 3D scenes using procedural generation techniques. This dedicated dataset would enable scalable training of neural rendering models and potentially resolve the current limitations in output fidelity.

## 7. Acknowledgment

We gratefully acknowledge UFIT Research Computing at the University of Florida and Stony Brook Research Computing and Cyberinfrastructure and the Institute for Advanced Computational Science at Stony Brook University for providing the computational resources and support that contributed to the research presented in this publication.

## References

- [1] Jonathan T Barron and Jitendra Malik. Shape, illumination, and reflectance from shading. *IEEE transactions on pattern analysis and machine intelligence*, 37(8):1670–1687, 2014. [1](#)
- [2] Harry Barrow, J Tenenbaum, A Hanson, and E Riseman. Recovering intrinsic scene characteristics. *Comput. vis. syst*, 2(3-26):2, 1978. [1](#), [3](#)
- [3] Anand Bhattad, Daniel McKee, Derek Hoiem, and David Forsyth. Stylegan knows normal, depth, albedo, and more. *Advances in Neural Information Processing Systems*, 36: 73082–73103, 2023. [3](#)
- [4] Andreas Blattmann, Tim Dockhorn, Sumith Kulal, Daniel Mendelevitch, Maciej Kilian, Dominik Lorenz, Yam Levi, Zion English, Vikram Voleti, Adam Letts, et al. Stable video diffusion: Scaling latent video diffusion models to large datasets. *arXiv preprint arXiv:2311.15127*, 2023. [2](#)
- [5] Tim Brooks, Aleksander Holynski, and Alexei A Efros. Instructpix2pix: Learning to follow image editing instructions. In *Proceedings of the IEEE/CVF conference on computer vision and pattern recognition*, pages 18392–18402, 2023. [2](#)
- [6] Chris Careaga and Yağız Aksoy. Intrinsic image decomposition via ordinal shading. *ACM Transactions on Graphics*, 43(1):1–24, 2023. [3](#)
- [7] Chris Careaga and Yağız Aksoy. Colorful diffuse intrinsic image decomposition in the wild. *ACM Transactions on Graphics (TOG)*, 43(6):1–12, 2024. [6](#), [7](#)
- [8] Duygu Ceylan, Chun-Hao P Huang, and Niloy J Mitra. Pix2video: Video editing using image diffusion. In *Proceedings of the IEEE/CVF International Conference on Computer Vision*, pages 23206–23217, 2023. [2](#)
- [9] Wenhao Chai, Xun Guo, Gaoang Wang, and Yan Lu. Stable-video: Text-driven consistency-aware diffusion video editing. In *Proceedings of the IEEE/CVF International Conference on Computer Vision*, pages 23040–23050, 2023.
- [10] Xi Chen, Lianghua Huang, Yu Liu, Yujun Shen, Deli Zhao, and Hengshuang Zhao. Anydoor: Zero-shot object-level image customization. In *Proceedings of the IEEE/CVF conference on computer vision and pattern recognition*, pages 6593–6602, 2024. [2](#)
- [11] Xi Chen, Sida Peng, Dongchen Yang, Yuan Liu, Bowen Pan, Chengfei Lv, and Xiaowei Zhou. Intrinsicanything: Learning diffusion priors for inverse rendering under unknown illumination. In *European Conference on Computer Vision*, pages 450–467. Springer, 2024. [7](#)
- [12] Yuren Cong, Mengmeng Xu, christian simon, Shoufa Chen, Jiawei Ren, Yanping Xie, Juan-Manuel Perez-Rua, Bodo Rosenhahn, Tao Xiang, and Sen He. FLATTEN: optical FLOW-guided ATTENTION for consistent text-to-video editing. In *The Twelfth International Conference on Learning Representations*, 2024. [5](#)
- [13] Xiaodan Du, Nicholas Kolkin, Greg Shakhnarovich, and Anand Bhattad. Generative models: What do they know? do they know things? let’s find out! *arXiv preprint arXiv:2311.17137*, 2023. [3](#), [8](#)
- [14] Patrick Esser, Sumith Kulal, Andreas Blattmann, Rahim Entezari, Jonas Müller, Harry Saini, Yam Levi, Dominik Lorenz, Axel Sauer, Frederic Boesel, et al. Scaling rectified flow transformers for high-resolution image synthesis. In *Forty-first international conference on machine learning*, 2024. [2](#)
- [15] Xiao Fu, Wei Yin, Mu Hu, Kaixuan Wang, Yuexin Ma, Ping Tan, Shaojie Shen, Dahua Lin, and Xiaoxiao Long. Geowizard: Unleashing the diffusion priors for 3d geometry estimation from a single image. In *European Conference on Computer Vision*, pages 241–258. Springer, 2024. [2](#)
- [16] Chen Geng, Hong-Xing Yu, Sharon Zhang, Maneesh Agrawala, and Jiajun Wu. Tree-structured shading decomposition. In *Proceedings of the IEEE/CVF International Conference on Computer Vision*, pages 488–498, 2023. [3](#)
- [17] Jia Gong, Lin Geng Foo, Zhipeng Fan, Qihong Ke, Hossein Rahmani, and Jun Liu. Diffpose: Toward more reliable 3d pose estimation. In *Proceedings of the IEEE/CVF Conference on Computer Vision and Pattern Recognition*, pages 13041–13051, 2023. [2](#)
- [18] David Griffiths, Tobias Ritschel, and Julien Philip. Outcast: Outdoor single-image relighting with cast shadows. In *Computer Graphics Forum*, pages 179–193. Wiley Online Library, 2022. [3](#)
- [19] Roger Grosse, Micah K Johnson, Edward H Adelson, and William T Freeman. Ground truth dataset and baseline evaluations for intrinsic image algorithms. In *2009 IEEE 12th International Conference on Computer Vision*, pages 2335–2342. IEEE, 2009. [1](#)
- [20] Ming Gui, Johannes Schusterbauer, Ulrich Prestel, Pingchuan Ma, Dmytro Kotovenko, Olga Grebenkova, Stefan Andreas Baumann, Vincent Tao Hu, and Björn Ommer. Depthfm: Fast monocular depth estimation with flow matching. *arXiv preprint arXiv:2403.13788*, 2024. [2](#)
- [21] Jing He, Haodong Li, Wei Yin, Yixun Liang, Leheng Li, Kaiqiang Zhou, Hongbo Zhang, Bingbing Liu, and Ying-Cong Chen. Lotus: Diffusion-based visual foundation model for high-quality dense prediction. *arXiv preprint arXiv:2409.18124*, 2024. [2](#), [6](#), [7](#)
- [22] Jonathan Ho and Tim Salimans. Classifier-free diffusion guidance. *arXiv preprint arXiv:2207.12598*, 2022. [2](#)
- [23] Jonathan Ho, Ajay Jain, and Pieter Abbeel. Denoising diffusion probabilistic models. *Advances in neural information processing systems*, 33:6840–6851, 2020. [2](#)
- [24] Jonathan Ho, Tim Salimans, Alexey Gritsenko, William Chan, Mohammad Norouzi, and David J Fleet. Video diffusion models. *Advances in Neural Information Processing Systems*, 35:8633–8646, 2022. [5](#)
- [25] Haian Jin, Yuan Li, Fujun Luan, Yuanbo Xiangli, Sai Bi, Kai Zhang, Zexiang Xu, Jin Sun, and Noah Snavely. Neural gaffer: Relighting any object via diffusion. *Advances in Neural Information Processing Systems*, 37:141129–141152, 2025. [2](#)
- [26] Tero Karras, Samuli Laine, and Timo Aila. A style-based generator architecture for generative adversarial networks. In *Proceedings of the IEEE/CVF conference on computer vision and pattern recognition*, pages 4401–4410, 2019. [3](#)
- [27] Bahjat Kawar, Shiran Zada, Oran Lang, Omer Tov, Huiwen Chang, Tali Dekel, Inbar Mosseri, and Michal Irani. Imagic:

- Text-based real image editing with diffusion models. In *Proceedings of the IEEE/CVF conference on computer vision and pattern recognition*, pages 6007–6017, 2023. 2
- [28] Bingxin Ke, Anton Obukhov, Shengyu Huang, Nando Metzger, Rodrigo Caye Daudt, and Konrad Schindler. Repurposing diffusion-based image generators for monocular depth estimation. In *Proceedings of the IEEE/CVF Conference on Computer Vision and Pattern Recognition*, pages 9492–9502, 2024. 2
- [29] Hoon Kim, Minje Jang, Wonjun Yoon, Jisoo Lee, Donghyun Na, and Sanghyun Woo. Switchlight: Co-design of physics-driven architecture and pre-training framework for human portrait relighting. In *Proceedings of the IEEE/CVF Conference on Computer Vision and Pattern Recognition*, pages 25096–25106, 2024. 3
- [30] Diederik P Kingma. Auto-encoding variational bayes. *arXiv preprint arXiv:1312.6114*, 2013. 3
- [31] Peter Kocsis, Vincent Sitzmann, and Matthias Nießner. Intrinsic image diffusion for single-view material estimation. *arXiv preprint arXiv:2312.12274*, 2023. 2, 3, 6, 7, 8
- [32] Peter Kocsis, Julien Philip, Kalyan Sunkavalli, Matthias Nießner, and Yannick Hold-Geoffroy. Lightit: Illumination modeling and control for diffusion models. In *Proceedings of the IEEE/CVF Conference on Computer Vision and Pattern Recognition*, pages 9359–9369, 2024. 2, 3
- [33] Balazs Kovacs, Sean Bell, Noah Snaveley, and Kavita Bala. Shading annotations in the wild. In *Proceedings of the IEEE conference on computer vision and pattern recognition*, pages 6998–7007, 2017. 3
- [34] Duong H Le, Tuan Pham, Sangho Lee, Christopher Clark, Aniruddha Kembhavi, Stephan Mandt, Ranjay Krishna, and Jiasen Lu. One diffusion to generate them all. *arXiv preprint arXiv:2411.16318*, 2024. 2
- [35] Junnan Li, Dongxu Li, Caiming Xiong, and Steven Hoi. Blip: Bootstrapping language-image pre-training for unified vision-language understanding and generation. In *International conference on machine learning*, pages 12888–12900. PMLR, 2022. 5
- [36] Junnan Li, Dongxu Li, Silvio Savarese, and Steven Hoi. Blip-2: Bootstrapping language-image pre-training with frozen image encoders and large language models. In *International conference on machine learning*, pages 19730–19742. PMLR, 2023. 5
- [37] Ming Li, Taojiannan Yang, Huafeng Kuang, Jie Wu, Zhaoning Wang, Xuefeng Xiao, and Chen Chen. Controlnet++: Improving conditional controls with efficient consistency feedback. In *European Conference on Computer Vision*, 2024. 2
- [38] Wenbin Li, Sajad Saeedi, John McCormac, Ronald Clark, Dimos Tzoumanikas, Qing Ye, Yuzhong Huang, Rui Tang, and Stefan Leutenegger. Interiornet: Mega-scale multi-sensor photo-realistic indoor scenes dataset. In *British Machine Vision Conference (BMVC)*, 2018. 3
- [39] Yixuan Li, Lihan Jiang, Linning Xu, Yuanbo Xiangli, Zhenzhi Wang, Dahua Lin, and Bo Dai. Matrixcity: A large-scale city dataset for city-scale neural rendering and beyond. In *Proceedings of the IEEE/CVF International Conference on Computer Vision*, pages 3205–3215, 2023. 2, 3, 5, 6, 7
- [40] Zhengqin Li, Mohammad Shafiei, Ravi Ramamoorthi, Kalyan Sunkavalli, and Manmohan Chandraker. Inverse rendering for complex indoor scenes: Shape, spatially-varying lighting and svbrdf from a single image. In *Proceedings of the IEEE/CVF conference on computer vision and pattern recognition*, pages 2475–2484, 2020. 2
- [41] Zhengqin Li, Ting-Wei Yu, Shen Sang, Sarah Wang, Meng Song, Yuhan Liu, Yu-Ying Yeh, Rui Zhu, Nitesh Gundavarapu, Jia Shi, et al. Openrooms: An open framework for photorealistic indoor scene datasets. In *Proceedings of the IEEE/CVF conference on computer vision and pattern recognition*, pages 7190–7199, 2021. 2, 3
- [42] Ruofan Liang, Zan Gojcic, Huan Ling, Jacob Munkberg, Jon Hasselgren, Zhi-Hao Lin, Jun Gao, Alexander Keller, Nandita Vijaykumar, Sanja Fidler, et al. Diffusionrenderer: Neural inverse and forward rendering with video diffusion models. *arXiv preprint arXiv:2501.18590*, 2025. 2, 3
- [43] Tsung-Yi Lin, Michael Maire, Serge Belongie, James Hays, Pietro Perona, Deva Ramanan, Piotr Dollár, and C Lawrence Zitnick. Microsoft coco: Common objects in context. In *Computer vision—ECCV 2014: 13th European conference, zurich, Switzerland, September 6–12, 2014, proceedings, part v 13*, pages 740–755. Springer, 2014. 5
- [44] Zhi-Hao Lin, Bohan Liu, Yi-Ting Chen, David Forsyth, Jia-Bin Huang, Anand Bhattad, and Shenlong Wang. Urbanir: Large-scale urban scene inverse rendering from a single video. *arXiv preprint arXiv:2306.09349*, 2023. 3
- [45] Shaoteng Liu, Yuechen Zhang, Wenbo Li, Zhe Lin, and Jiaya Jia. Video-p2p: Video editing with cross-attention control. In *Proceedings of the IEEE/CVF Conference on Computer Vision and Pattern Recognition*, pages 8599–8608, 2024. 2
- [46] Jundan Luo, Duygu Ceylan, Jae Shin Yoon, Nanxuan Zhao, Julien Philip, Anna Frühstück, Wenbin Li, Christian Richardt, and Tuanfeng Wang. Intrinsicdiffusion: Joint intrinsic layers from latent diffusion models. In *ACM SIGGRAPH 2024 Conference Papers*, pages 1–11, 2024. 2, 3
- [47] Gonzalo Martin Garcia, Karim Abou Zeid, Christian Schmidt, Daan de Geus, Alexander Hermans, and Bastian Leibe. Fine-tuning image-conditional diffusion models is easier than you think. In *Proceedings of the IEEE/CVF Winter Conference on Applications of Computer Vision (WACV)*, 2025. 1, 2, 3, 4, 6, 7
- [48] Chong Mou, Xintao Wang, Liangbin Xie, Yanze Wu, Jian Zhang, Zhongang Qi, and Ying Shan. T2i-adapter: Learning adapters to dig out more controllable ability for text-to-image diffusion models. In *Proceedings of the AAAI conference on artificial intelligence*, pages 4296–4304, 2024. 2
- [49] Oliver Nalbach, Elena Arabadzhiyska, Dushyant Mehta, H-P Seidel, and Tobias Ritschel. Deep shading: convolutional neural networks for screen space shading. In *Computer graphics forum*, pages 65–78. Wiley Online Library, 2017. 3
- [50] Rohit Pandey, Sergio Orts-Escolano, Chloe Legendre, Christian Haene, Sofien Bouaziz, Christoph Rhemann, Paul E Debevec, and Sean Ryan Fanello. Total relighting: learning to relight portraits for background replacement. *ACM Trans. Graph.*, 40(4):43–1, 2021. 3



- [51] Matt Pharr, Wenzel Jakob, and Greg Humphreys. *Physically based rendering: From theory to implementation*. MIT Press, 2023. 2, 3
- [52] Julien Philip, Michaël Gharbi, Tinghui Zhou, Alexei A Efros, and George Drettakis. Multi-view relighting using a geometry-aware network. *ACM Trans. Graph.*, 38(4):78–1, 2019. 3
- [53] Bryan A Plummer, Liwei Wang, Chris M Cervantes, Juan C Caicedo, Julia Hockenmaier, and Svetlana Lazebnik. Flickr30k entities: Collecting region-to-phrase correspondences for richer image-to-sentence models. In *Proceedings of the IEEE international conference on computer vision*, pages 2641–2649, 2015. 5
- [54] Can Qin, Shu Zhang, Ning Yu, Yihao Feng, Xinyi Yang, Yingbo Zhou, Huan Wang, Juan Carlos Niebles, Caiming Xiong, Silvio Savarese, et al. Unicontrol: A unified diffusion model for controllable visual generation in the wild. *arXiv preprint arXiv:2305.11147*, 2023. 2
- [55] Alexander Raistrick, Lahav Lipson, Zeyu Ma, Lingjie Mei, Mingzhe Wang, Yiming Zuo, Karhan Kayan, Hongyu Wen, Beining Han, Yihan Wang, Alejandro Newell, Hei Law, Ankit Goyal, Kaiyu Yang, and Jia Deng. Infinite photorealistic worlds using procedural generation. In *Proceedings of the IEEE/CVF Conference on Computer Vision and Pattern Recognition*, pages 12630–12641, 2023. 2
- [56] Alexander Raistrick, Lingjie Mei, Karhan Kayan, David Yan, Yiming Zuo, Beining Han, Hongyu Wen, Meenal Parakh, Stamatis Alexandropoulos, Lahav Lipson, Zeyu Ma, and Jia Deng. Infinigen indoors: Photorealistic indoor scenes using procedural generation. In *Proceedings of the IEEE/CVF Conference on Computer Vision and Pattern Recognition (CVPR)*, pages 21783–21794, 2024. 2
- [57] Ravi Ramamoorthi and Pat Hanrahan. A signal-processing framework for inverse rendering. In *Proceedings of the 28th annual conference on Computer graphics and interactive techniques*, pages 117–128, 2001. 1
- [58] Mani Ramanagopal, Sriram Narayanan, Aswin C Sankaranarayanan, and Srinivasa G Narasimhan. A theory of joint light and heat transport for lambertian scenes. In *Proceedings of the IEEE/CVF Conference on Computer Vision and Pattern Recognition*, pages 11924–11933, 2024. 3
- [59] René Ranftl, Katrin Lasinger, David Hafner, Konrad Schindler, and Vladlen Koltun. Towards robust monocular depth estimation: Mixing datasets for zero-shot cross-dataset transfer. *IEEE transactions on pattern analysis and machine intelligence*, 44(3):1623–1637, 2020. 4
- [60] Mengwei Ren, Wei Xiong, Jae Shin Yoon, Zhixin Shu, Jianming Zhang, HyunJoon Jung, Guido Gerig, and He Zhang. Relightful harmonization: Lighting-aware portrait background replacement. In *Proceedings of the IEEE/CVF Conference on Computer Vision and Pattern Recognition*, pages 6452–6462, 2024. 2
- [61] Mike Roberts, Jason Ramapuram, Anurag Ranjan, Atulit Kumar, Miguel Angel Bautista, Nathan Paczan, Russ Webb, and Joshua M Susskind. Hypersim: A photorealistic synthetic dataset for holistic indoor scene understanding. In *Proceedings of the IEEE/CVF international conference on computer vision*, pages 10912–10922, 2021. 2, 3, 5, 6, 7, 9
- [62] Robin Rombach, Andreas Blattmann, Dominik Lorenz, Patrick Esser, and Björn Ommer. High-resolution image synthesis with latent diffusion models. In *Proceedings of the IEEE/CVF conference on computer vision and pattern recognition*, pages 10684–10695, 2022. 2, 3
- [63] Viktor Rudnev, Mohamed Elgharib, William Smith, Lingjie Liu, Vladislav Golyanik, and Christian Theobalt. Nerf for outdoor scene relighting. In *European Conference on Computer Vision*, pages 615–631. Springer, 2022. 3
- [64] Chitwan Saharia, William Chan, Saurabh Saxena, Lala Li, Jay Whang, Emily L Denton, Kamyar Ghasemipour, Raphael Gontijo Lopes, Burcu Karagol Ayan, Tim Salimans, et al. Photorealistic text-to-image diffusion models with deep language understanding. *Advances in neural information processing systems*, 35:36479–36494, 2022. 2
- [65] Tim Salimans and Jonathan Ho. Progressive distillation for fast sampling of diffusion models. *arXiv preprint arXiv:2202.00512*, 2022. 3, 4
- [66] Wen Wang, Canyu Zhao, Hao Chen, Zhekai Chen, Kecheng Zheng, and Chunhua Shen. Autostory: Generating diverse storytelling images with minimal human efforts. *International Journal of Computer Vision*, pages 1–22, 2024. 2
- [67] Zian Wang, Tianchang Shen, Jun Gao, Shengyu Huang, Jacob Munkberg, Jon Hasselgren, Zan Gojcic, Wenzheng Chen, and Sanja Fidler. Neural fields meet explicit geometric representations for inverse rendering of urban scenes. In *Proceedings of the IEEE/CVF Conference on Computer Vision and Pattern Recognition*, pages 8370–8380, 2023. 3
- [68] Zhaoqing Wang, Xiaobo Xia, Runnan Chen, Dongdong Yu, Changhu Wang, Mingming Gong, and Tongliang Liu. Lavindit: Large vision diffusion transformer. *arXiv preprint arXiv:2411.11505*, 2024. 2
- [69] Jiaye Wu, Sanjoy Chowdhury, Hariharmano Shanmugaraja, David Jacobs, and Soumyadip Sengupta. Measured albedo in the wild: Filling the gap in intrinsics evaluation. In *2023 IEEE International Conference on Computational Photography (ICCP)*, pages 1–12. IEEE, 2023. 3
- [70] Tong Wu, Jia-Mu Sun, Yu-Kun Lai, Yuewen Ma, Leif Kobbelt, and Lin Gao. Deferredreds: Decoupled and editable gaussian splatting with deferred shading. *arXiv preprint arXiv:2404.09412*, 2024. 3
- [71] Guangkai Xu, Yongtao Ge, Mingyu Liu, Chengxiang Fan, Kangyang Xie, Zhiyue Zhao, Hao Chen, and Chunhua Shen. What matters when repurposing diffusion models for general dense perception tasks? *arXiv preprint arXiv:2403.06090*, 2024. 2
- [72] Binxin Yang, Shuyang Gu, Bo Zhang, Ting Zhang, Xuejin Chen, Xiaoyan Sun, Dong Chen, and Fang Wen. Paint by example: Exemplar-based image editing with diffusion models. In *Proceedings of the IEEE/CVF conference on computer vision and pattern recognition*, pages 18381–18391, 2023. 2
- [73] Chongjie Ye, Lingteng Qiu, Xiaodong Gu, Qi Zuo, Yushuang Wu, Zilong Dong, Liefeng Bo, Yuliang Xiu, and Xiaoguang Han. Stablenormal: Reducing diffusion variance for stable and sharp normal. *ACM Transactions on Graphics (TOG)*, 43(6):1–18, 2024. 2, 6, 7



- [74] Hu Ye, Jun Zhang, Sibao Liu, Xiao Han, and Wei Yang. Ip-adapter: Text compatible image prompt adapter for text-to-image diffusion models. *arXiv preprint arXiv:2308.06721*, 2023. [2](#)
- [75] Weicai Ye, Shuo Chen, Chong Bao, Hujun Bao, Marc Pollefeys, Zhaopeng Cui, and Guofeng Zhang. Intrinsicnerf: Learning intrinsic neural radiance fields for editable novel view synthesis. In *Proceedings of the IEEE/CVF International Conference on Computer Vision*, pages 339–351, 2023. [3](#)
- [76] Yusaku Yoshida, Ryo Kawahara, and Takahiro Okabe. Light source separation and intrinsic image decomposition under ac illumination. In *Proceedings of the IEEE/CVF Conference on Computer Vision and Pattern Recognition*, pages 5735–5743, 2023. [3](#)
- [77] Ye Yu, Abhimitra Meka, Mohamed Elgharib, Hans-Peter Seidel, Christian Theobalt, and William AP Smith. Self-supervised outdoor scene relighting. In *Computer Vision—ECCV 2020: 16th European Conference, Glasgow, UK, August 23–28, 2020, Proceedings, Part XXII 16*, pages 84–101. Springer, 2020. [3](#)
- [78] Chong Zeng, Yue Dong, Pieter Peers, Youkang Kong, Hongzhi Wu, and Xin Tong. Dilightnet: Fine-grained lighting control for diffusion-based image generation. In *ACM SIGGRAPH 2024 Conference Papers*, pages 1–12, 2024. [2](#)
- [79] Zheng Zeng, Valentin Deschaintre, Iliyan Georgiev, Yannick Hold-Geoffroy, Yiwei Hu, Fujun Luan, Ling-Qi Yan, and Miloš Hašan. Rgb $\leftrightarrow$ x: Image decomposition and synthesis using material- and lighting-aware diffusion models. In *ACM SIGGRAPH 2024 Conference Papers*, New York, NY, USA, 2024. Association for Computing Machinery. [1](#), [2](#), [3](#), [5](#), [6](#), [7](#), [8](#)
- [80] Lvmin Zhang, Anyi Rao, and Maneesh Agrawala. Adding conditional control to text-to-image diffusion models. In *Proceedings of the IEEE/CVF international conference on computer vision*, pages 3836–3847, 2023. [2](#)
- [81] Lvmin Zhang, Anyi Rao, and Maneesh Agrawala. Scaling in-the-wild training for diffusion-based illumination harmonization and editing by imposing consistent light transport. In *The Thirteenth International Conference on Learning Representations*, 2025. [2](#)
- [82] Zitian Zhang, Frédéric Fortier-Chouinard, Mathieu Garon, Anand Bhattad, and Jean-François Lalonde. Zerocomp: Zero-shot object compositing from image intrinsics via diffusion. *arXiv preprint arXiv:2410.08168*, 2024. [3](#)
- [83] Tinghui Zhou, Philipp Krahenbuhl, and Alexei A Efros. Learning data-driven reflectance priors for intrinsic image decomposition. In *Proceedings of the IEEE international conference on computer vision*, pages 3469–3477, 2015. [3](#)
- [84] Yupeng Zhou, Daquan Zhou, Ming-Ming Cheng, Jiashi Feng, and Qibin Hou. Storydiffusion: Consistent self-attention for long-range image and video generation. *Advances in Neural Information Processing Systems*, 37: 110315–110340, 2025. [2](#)
- [85] Jingsen Zhu, Fujun Luan, Yuchi Huo, Zihao Lin, Zhihua Zhong, Dianbing Xi, Rui Wang, Hujun Bao, Jiaxiang Zheng, and Rui Tang. Learning-based inverse rendering of complex indoor scenes with differentiable monte carlo raytracing. In *SIGGRAPH Asia 2022 Conference Papers*, pages 1–8, 2022. [1](#), [2](#), [3](#), [5](#), [6](#), [7](#), [8](#), [9](#)
- [86] Jun-Yan Zhu, Taesung Park, Phillip Isola, and Alexei A Efros. Unpaired image-to-image translation using cycle-consistent adversarial networks. In *Proceedings of the IEEE international conference on computer vision*, pages 2223–2232, 2017. [2](#), [5](#)
- [87] Muzhi Zhu, Yang Liu, Zekai Luo, Chenchen Jing, Hao Chen, Guangkai Xu, Xinlong Wang, and Chunhua Shen. Unleashing the potential of the diffusion model in few-shot semantic segmentation. *arXiv preprint arXiv:2410.02369*, 2024. [2](#)
- [88] Rui Zhu, Zhengqin Li, Janarбек Matai, Fatih Porikli, and Manmohan Chandraker. Irisformer: Dense vision transformers for single-image inverse rendering in indoor scenes. In *Proceedings of the IEEE/CVF Conference on Computer Vision and Pattern Recognition*, pages 2822–2831, 2022. [2](#)
- [89] Daniel Zoran, Phillip Isola, Dilip Krishnan, and William T Freeman. Learning ordinal relationships for mid-level vision. In *Proceedings of the IEEE international conference on computer vision*, pages 388–396, 2015. [3](#)